

# Frozen Backpropagation: Relaxing Weight Symmetry in Temporally-Coded Deep Spiking Neural Networks

Gaspard Goupy<sup>1</sup>, Pierre Tirilly<sup>1</sup>, and Ioan Marius Bilasco<sup>1,\*</sup>

<sup>1</sup>Univ. Lille, CNRS, Centrale Lille, UMR 9189 CRISTAL, F-59000 Lille, France

\*Corresponding author: marius.bilasco@univ-lille.fr

## Abstract

Direct training of Spiking Neural Networks (SNNs) on neuromorphic hardware can greatly reduce energy costs compared to GPU-based training. However, implementing Backpropagation (BP) on such hardware is challenging because forward and backward passes are typically performed by separate networks with distinct weights. To compute correct gradients, forward and feedback weights must remain symmetric during training, necessitating weight transport between the two networks. This symmetry requirement imposes hardware overhead and increases energy costs. To address this issue, we introduce Frozen Backpropagation (FBP), a BP-based training algorithm relaxing weight symmetry in settings with separate networks. FBP updates forward weights by computing gradients with periodically frozen feedback weights, reducing weight transports during training and minimizing synchronization overhead. To further improve transport efficiency, we propose three partial weight transport schemes of varying computational complexity, where only a subset of weights is transported at a time. We evaluate our methods on image recognition tasks and compare them to existing approaches addressing the weight symmetry requirement. Our results show that FBP outperforms these methods and achieves accuracy comparable to BP. With partial weight transport, FBP can substantially lower transport costs by  $1,000\times$  with an accuracy drop of only 0.5 pp on CIFAR-10 and 1.1 pp on CIFAR-100, or by up to  $10,000\times$  at the expense of moderated accuracy loss. This work provides insights for guiding the design of neuromorphic hardware incorporating BP-based on-chip learning.

## 1 Introduction

Spiking Neural Networks (SNNs) are a promising alternative to second-generation Artificial Neural Networks (ANNs) for energy-efficient computing [1]. Coupled with neuromorphic hardware [2], which supports highly parallel processing and in-memory computing, SNNs can overcome the von Neumann bottleneck and reduce energy consumption by orders of magnitude compared to conventional CPU/GPU-based platforms [3, 4, 5]. To unlock their energy-efficient potential and facilitate hardware deployment, neuromorphic chips should incorporate scalable on-chip learning [6].

State-of-the-art training methods for SNNs are based on Backpropagation (BP) [7], with Backpropagation Through Time (BPTT) being the most effective approach [8, 9]. However, BPTT is very demanding in terms of computation and memory [10], and typically optimizes spike counts, ignoring the temporal information carried by spikes [6]. In contrast, event-driven BP for networks using Time-to-First-Spike (TTFS) coding [11], a form of temporal coding, enables more efficient BP training [12, 13, 14, 6]. TTFS encodes information in spike timings by limiting each neuron to a single spike per sample. TTFS-based SNNs present several advantages, including exact gradient computation [6], energy efficiency [15], low latency [16], and high information capacity [17].

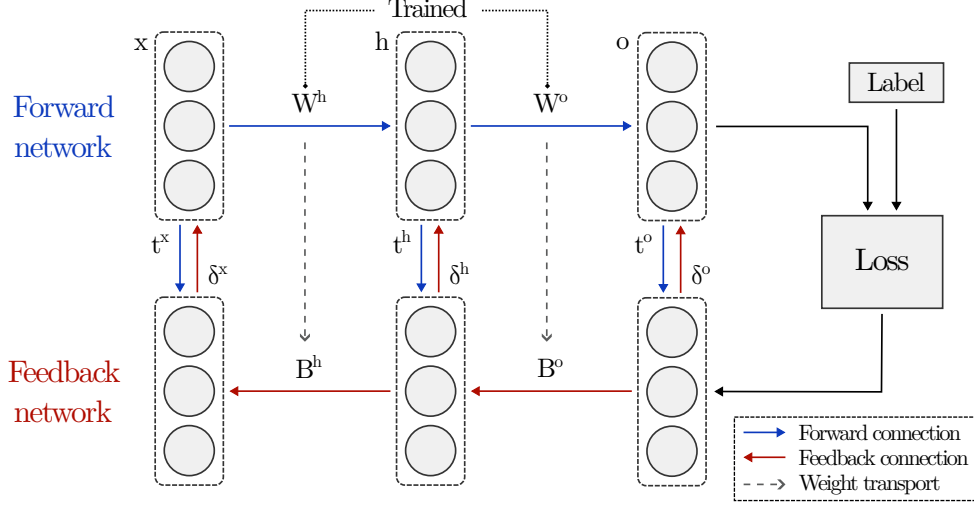


Figure 1: BP-based training in a dual-network configuration, consisting of a forward and a feedback network with distinct, unidirectional synapses. The forward network uses weights  $W$  to compute neuron spike times  $t$ . The feedback network uses weights  $B$  to compute neuron errors  $\delta$ . Neuron errors act as feedback signals triggering weight updates only in the forward network. For correct gradient computation, weight transport is needed to maintain  $B$  symmetric with  $W$  during training.

Despite their success in training SNNs, BP-based algorithms remain challenging to implement on neuromorphic hardware [18, 19, 20]. One key challenge is that neuromorphic hardware typically uses unidirectional synapses (like biological systems), requiring separate networks with distinct weights for the forward and backward passes [20]. We refer to this setup as dual-network configuration, illustrated in Figure 1. In this setup, only the forward weights are updated, based on neuron errors computed with the feedback weights. To ensure correct credit assignment, the feedback weights must remain perfectly symmetric with the forward weights during training, which requires realignment after each iteration (i.e., each update of the forward weights). This issue, known as the weight transport problem [21, 22, 20], or the weight symmetry requirement [23, 24], is both challenging and costly due to increased circuitry and energy costs associated with data movement [25, 19].

Several alternatives to BP have been explored to eliminate or reduce the need for weight transport [26, 27, 28, 29, 30]. Among them, feedback-driven methods [31, 32, 33, 22] are particularly attractive because they enable BP-like training. Feedback Alignment (FA) [31] eliminates weight transport by propagating errors through fixed, random feedback matrices instead of the exact transpose of the forward weights. FA and its variants have been widely studied for training shallow SNNs [18, 34, 35, 36]. However, studies on ANNs have shown that it struggles to scale to deeper networks [37, 38, 33], unless sign symmetry between forward and feedback weights is enforced, as in Sign-concordant Feedback Alignment (sFA) [23, 38]. To date, sFA has only been applied to ANNs. Alternatively, Sign-Symmetry (SS) [33] offers a relaxed form of weight symmetry, where the feedback weights are reduced to the sign of the forward weights. This approach scales better to deeper ANN networks than FA [33], but it still relies on sign transport to maintain sign symmetry, similar to sFA. Exploration of SS in SNNs is limited; to our knowledge, only one study has used it, for continual learning [39]. In summary, SS and sFA offer simple and relatively scalable alternatives to exact weight symmetry when relying on sign transport. However, their application to deep SNNs remains largely unexplored. In addition, the magnitude mismatch between forward and feedback weights inevitably introduces bias, distorting the direction of the gradients. To better approximate the gradient directions of BP, there is a need for methods that relax weight symmetry while minimizing this magnitude mismatch.

In this paper, we address weight symmetry in TTFS-based deep SNNs under dual-network configurations. We aim to improve training efficiency by reducing the frequency of weight transport and minimizing the synchronization overhead between the forward and feedback networks. Our main contributions can be summarized as follows:

1. We introduce Frozen Backpropagation (FBP), a BP-based training algorithm that reduces the frequency of weight transport by updating forward weights using gradients computed from frozen

feedback weights. At fixed intervals, the forward weights are transported to realign the feedback weights, minimizing magnitude mismatch and preserving gradient direction.

2. To further optimize transport efficiency, we propose a partial weight transport scheme where only a subset of the weights is transported at a time. We design three selection strategies of varying computational complexities.
3. We benchmark sFA and SS for the first time in TTFS-based deep SNNs. We show that FBP outperforms these methods on image recognition tasks and achieves accuracy comparable to BP. Also, we study the trade-off between transport efficiency and accuracy: with partial weight transport, FBP lowers transport costs by  $1,000\times$  with an accuracy drop of only 0.5 pp on CIFAR-10 and 1.1 pp on CIFAR-100, or by up to  $10,000\times$  at the expense of moderated accuracy loss.

This work provides insights to guide future efforts in designing neuromorphic hardware with efficient BP-based on-chip learning. The source code is publicly available at: <https://gitlab.univ-lille.fr/fox/fbp>.

## 2 Preliminaries

### 2.1 TTFS-Based Deep SNN Baseline

Our work builds upon the TTFS-based deep SNN introduced in [14], selected for its state-of-the-art performance and training efficiency. This framework features TTFS coding, single-spike Rectified Linear Postsynaptic Potential (ReL-PSP) neurons, non-overlapping spike time windows, and event-driven BP algorithm. Full specifications and motivations are provided in Appendix A.

Training TTFS-based SNNs using BP involves computing gradients with respect to spike times:

$$\frac{\partial \mathcal{L}}{\partial W^l} = \underbrace{\frac{\partial \mathcal{L}}{\partial t^L} \frac{\partial t^L}{\partial t^{L-1}} \cdots \frac{\partial t^{l+1}}{\partial t^l}}_{\delta^l} \frac{\partial t^l}{\partial W^l}, \quad (1)$$

where  $t^l$  are the spike times of layer  $l$ ,  $W^l$  are the weights of layer  $l$ ,  $L$  is the output layer, and  $\mathcal{L}$  is the loss. We refer to  $\delta^l = \frac{\partial \mathcal{L}}{\partial t^l}$  as the neuron errors, which is the gradient of the loss with respect to the spike times of neurons in layer  $l$ . The expressions for the partial derivatives in Equation 1 depend on the specific SNN model used; full derivations for our baseline are included in Appendix A.3.

### 2.2 BP-Based Training in Dual-Network Configurations

In a dual-network configuration (Figure 1), forward and backward passes are computed by two networks with distinct weights: a forward network with weights  $W$ , and a feedback network with weights  $B$ . Algorithm 1 provides a high-level overview of how training is carried out. Note that the forward network shares spike times with the feedback network to compute neuron errors, while the feedback network shares neuron errors with the forward network to compute weight changes.

The weight symmetry requirement for correct gradient propagation demands weight transport between forward and feedback weights. This transport is performed by copying  $W$  to  $B$  after each iteration (i.e., after each update of  $W$ ), implemented through the `WEIGHTTRANSPORT` function in step 14. Several approaches have been proposed to relax this constraint; below, we formally describe two main feedback-driven methods.

**Feedback Alignment** FA eliminates weight symmetry by defining  $B$  as a fixed, random matrix. To improve scalability to deeper networks, the sFA variant preserves the sign of the forward weights in the feedback path, removing weight transport but introducing sign transport instead. In this case,  $B = \hat{B} \circ \text{sign}(W)$ , where  $\hat{B}$  is initialized once and fixed throughout training,  $\text{sign}(\cdot)$  is the element-wise sign function, and  $\circ$  is element-wise multiplication. This approach can be implemented by modifying the `WEIGHTTRANSPORT` function to update the signs of  $B$  to match those of  $W$ .

**Sign-Symmetry** SS reduces  $B$  to the sign of  $W$ :  $B = \text{sign}(W)$ . Similar to sFA, sign transport is required to maintain sign symmetry throughout training, which can be implemented by modifying the `WEIGHTTRANSPORT` function as above. Unlike sFA, however, SS eliminates stochasticity, since the feedback weights are restricted to either  $+1$  or  $-1$ .

---

**Algorithm 1** BP training in a dual-network configuration

---

```
1: FN: Forward Network; BN: Feedback Network
2: for each iteration  $i$  do
3:   for  $l = 1$  to  $L$  do
4:     (FN) Compute spike times  $t^l$  with  $W^l$  ▷ Eq A.5
5:     (FN) Send  $t^l$  to the corresponding feedback layer
6:   end for
7:   Compute loss  $\mathcal{L}$  from  $t^L$  ▷ Eq A.6
8:   for  $l = L$  to  $1$  do
9:     (BN) Compute neuron errors  $\delta^l$  with  $B^l$  ▷ Eq A.8
10:    (BN) Send  $\delta^l$  to the corresponding forward layer
11:    (FN) Compute  $\frac{\partial t^l}{\partial W^l}$  with  $W^l$  ▷ Eq A.7
12:    (FN) Update  $W^l$  with  $\delta^l$  and  $\frac{\partial t^l}{\partial W^l}$  ▷ Eq 1
13:  end for
14:  (FN) WEIGHTTRANSPORT( $W, B, i$ )
15: end for
```

---

### 3 Methods

#### 3.1 Frozen Backpropagation

Frozen Backpropagation (FBP) is a modified BP algorithm designed to operate in the dual-network configuration described in Section 2.2, with distinct forward and feedback networks. Unlike conventional BP, which enforces strict weight symmetry between the forward weights  $W$  and the feedback weights  $B$  through weight transport after each iteration, FBP relaxes this requirement by decoupling the update schedules of the two networks. Specifically,  $W$  is updated after each iteration (i.e., after each backward pass), while  $B$  is kept frozen for a fixed number of iterations  $\Phi$ . As training progresses, the symmetry between  $W$  and  $B$  is gradually broken, with neuron errors computed using a stale copy of  $W$ . After  $\Phi$  iterations, the weights are realigned by copying (i.e., transporting)  $W$  to  $B$ , restoring symmetry. This transport, illustrated in Figure 1, is implemented in Algorithm 1 by modifying the WEIGHTTRANSPORT function to occur every  $\Phi$  iterations. Therefore, FBP reduces the frequency of weight transport during training, which may improve energy efficiency by reducing data movement and memory accesses. It may also lower training latency by eliminating the synchronization overhead between forward and feedback weights after each iteration. The hyperparameter  $\Phi$  determines the number of iterations between weight transports and thus directly translates to the transport reduction factor relative to BP, assuming an equal number of training epochs. For example,  $\Phi = 10$  reduces the per-epoch transport frequency by a factor of 10. As such,  $\Phi$  controls the accuracy-efficiency trade-off in FBP: larger values improve efficiency by reducing weight transport frequency but also increase gradient bias in later iterations, which may ultimately degrade performance. Note that FBP is agnostic to the SNN model and the BP algorithm, as it intervenes solely in the weight transport step. In principle, it can be applied with BPTT or even with SS, by transporting only the updated signs. Also, FBP introduces no computational overhead compared to BP.

Previous work [31, 33] showed that exact symmetry between forward and feedback weights is not essential for scalable BP-based learning; preserving only the sign of the weights can be sufficient. However, such relaxed constraints may lead to suboptimal training when the weight magnitudes differ too much. For instance, a forward weight of 0.01 and a feedback weight of 0.99 have the same sign, but the large difference causes the corresponding input neuron to be treated very differently during learning. In the forward network, the neuron has little influence on the output spike, while in the feedback network, it is mistakenly seen as a strong contributor during error propagation. This magnitude mismatch alters the direction of the feedback signal, leading to inaccurate gradient estimates. The purpose of FBP is to minimize this mismatch by periodically transporting weights from  $W$  to  $B$ , ensuring that forward and feedback weights share not only the same sign but also a consistent estimate of each neuron’s contribution.

#### 3.2 Partial Weight Transport

FBP transports weights from  $W$  to  $B$  every  $\Phi$  iterations to correct the gradient bias introduced by  $B$ . A question arises: *What is the minimal number of weights that must be transported to sufficiently*

*correct the bias?* Transporting only a subset of the weights every  $\Phi$  iterations could further reduce transport costs and improve energy efficiency. Based on this observation, we propose a partial weight transport scheme with three weight selection strategies of varying complexity.

**Top-K Largest Change** Bias arises when a weight value in  $W$  deviates too much from its counterpart in  $B$ . Moreover, larger deviations contribute to larger bias. An effective strategy is to, every  $\Phi$  iterations, select for each layer  $l$  the top  $K\%$  of weights in  $W^l$  with the largest absolute changes since the last transport. This can be formalized as:

$$\begin{aligned}\Delta_{ij}^l &= |W_{ij}^l - \widetilde{W}_{ij}^l|, \\ B_{ij}^l &= \begin{cases} W_{ij}^l & \text{if } \Delta_{ij}^l \geq \tau^l, \\ B_{ij}^l & \text{o.w.} \end{cases},\end{aligned}\tag{2}$$

where  $\widetilde{W}_{ij}^l$  is the value of the forward weight between neuron  $n_i^{l-1}$  and  $n_j^l$  at the time of its last transport, and  $\tau^l$  is the threshold corresponding to the top  $K\%$  of  $\Delta_{ij}^l$  values. Determining  $\tau^l$  requires layer-level computation (not local to the synapse), and its complexity scales linearly with the number of weights. This method effectively corrects larger biases but incurs additional computational and memory overhead in the forward network, as it involves finding  $\tau^l$  and storing previous weight values.

**Random Sampling** A low-complexity and hardware-friendlier alternative is to randomly sample weights for transport. Every  $\Phi$  iterations, each weight in  $W$  is transported with a fixed probability  $P$  (Bernoulli sampling). This method assumes that randomly sampling weights with a sufficiently high  $P$  is enough to adequately correct the bias over time. However, it does not guarantee immediate correction of larger biases. Since the probability is applied at the synapse level, it incurs no additional non-local computation or significant memory overhead.

**Change-Weighted Sampling** To correct larger biases while avoiding non-local computation, we build upon the two previous strategies by sampling weights based on the magnitude of their changes. Unlike the previous strategies, this method does not transport the weights at a fixed interval  $\Phi$  but instead allows each forward weight to determine when to transport its value (hence,  $\Phi$  is set to 1). The probability  $P_{ij}^l$  of transporting a weight  $W_{ij}^l$  after an iteration is:

$$\begin{aligned}P_{ij}^l &= 1 - \exp\left(-\frac{|W_{ij}^l - \widetilde{W}_{ij}^l|}{\beta}\right), \\ B_{ij}^l &= \begin{cases} W_{ij}^l & \text{with probability } P_{ij}^l, \\ B_{ij}^l & \text{o.w.} \end{cases},\end{aligned}\tag{3}$$

where  $\beta$  is a temperature parameter controlling the sharpness of the selection probability.  $\beta$  is a substitute for the fixed interval  $\Phi$  since it indirectly controls transport frequency: the lower  $\beta$ , the more frequently weights are realigned. Removing the need for a fixed interval allows this method to adapt more effectively to significant weight changes, which would otherwise require waiting for  $\Phi$  iterations before being corrected. In addition, it simplifies the tuning process, as it only requires a single hyperparameter ( $\beta$ ) instead of two ( $\Phi$ , and  $K$  or  $P$ ). A drawback of this method is the additional memory required in the forward network to store previous weight values.

## 4 Results

### 4.1 Experimental Setup

In this section, we describe the experimental setup used to evaluate our approach. Additional details are provided in Appendix B.1.

**Datasets** We select three image recognition datasets of increasing complexity: Fashion-MNIST [40], CIFAR-10 [41], and CIFAR-100 [41]. Fashion-MNIST is a more challenging variant of MNIST [42], comprising  $28 \times 28$  grayscale images, 60,000 samples for training and 10,000 for testing, categorized into 10 classes. CIFAR-10 and CIFAR-100 contain  $32 \times 32$  RGB images, with 50,000 training samples and 10,000 test samples. They consist of 10 and 100 classes, respectively.

**Architectures** We evaluate our methods on two VGG-based architectures [43]: VGG-7 and VGG-11. We do not consider deeper variants such as VGG-16 due to the increased difficulty of parameter initialization, which prior work typically addresses through ANN pretraining [14, 6]. Our VGG-7 structure is  $64C3 - 128C3 - P2 - 256C3 - 256C3 - P2 - 512C3 - 512C3 - P2$ , while VGG-11 is  $128C3 - 128C3 - 128C3 - P2 - 256C3 - 256C3 - 256C3 - P2 - 512C3 - 512C3 - 512C3 - 512C3 - P2$ . For convolutional layers ( $XC3$ ),  $X$  denotes the number of channels and 3 the kernel size. The stride is always 1, and zero-padding is applied to preserve spatial dimensions. For pooling layers ( $P2$ ), we use max-pooling with a kernel of size 2, stride of 2, and no padding. Both architectures are followed by a fully-connected layer, with the number of neurons matching the number of classes. We use Kaiming initialization [44], and do not add bias terms to reduce model complexity.

**Protocol** We employ the Adam optimizer [45] ( $\alpha = 10^{-4}$ ,  $\beta_1 = 0.9$ , and  $\beta_2 = 0.999$ ), L2 regularization ( $\lambda = 10^{-1}$ ), gradient clipping (threshold of 1), and annealing of the learning rate ( $\alpha$ ) after each epoch (factor of 0.999). We train the networks with a batch size of 256, and we apply early stopping with a patience of 25 epochs. Input images are normalized to  $[0, 1]$ . For CIFAR-10 and CIFAR-100, we employ data augmentation following the approach in [14] to mitigate overfitting. 10% of the training set is randomly reserved for validation (random holdout split). Results on test sets are averaged over 8 trials with different random initializations; we report the mean and one standard deviation. The network architectures and the hyperparameters ( $\alpha$ ,  $\lambda$ , gradient clipping, and annealing) were optimized for BP training on the validation set of CIFAR-10 using a gridsearch algorithm.

## 4.2 Comparison with Existing Methods

We compare, in Table 1, the performance of FBP against BP, along with sFA and SS. In BP, weight signs and values are transported after each iteration (every 256 samples). For sFA and SS, only weight signs are transported after each iteration. In FBP,  $\Phi$  is set to enable the transport of signs and values at a frequency of 0.1 ( $\Phi = 10$ ). Thus, for a given epoch, weight transport occurs 10% of the time compared to its alternatives. We selected the highest  $\Phi$  maintaining, on average, optimal validation performance on CIFAR-10. For this comparison, we consider FBP without partial weight transport.

Our method, FBP, achieves test accuracy comparable to BP across all datasets and network architectures, while reducing weight transport per epoch by  $10\times$ . Note that BP typically converges in fewer epochs on CIFAR-10 and CIFAR-100 (in average, 9% fewer epochs), leading to a minor reduction in total weight transports. However, this reduction is largely offset by the substantial savings achieved per epoch in FBP. For instance, on CIFAR-10 with the VGG-7 architecture—where BP requires 11% fewer epochs to converge—we measure 46,112 weight transports with BP over 262 epochs, compared to only 5,192 with FBP over 295 epochs ( $8.9\times$  reduction over the full training).

FBP outperforms existing feedback-driven methods relaxing weight symmetry through sign transport. sFA performs significantly worse than all other methods, confirming that stochasticity prevents scalability in deeper networks. This aligns with prior studies on traditional ANNs [37, 38, 33], though, to our knowledge, it has never been demonstrated in SNNs. SS provides a more effective alternative to sFA, achieving accuracy closer to the BP baseline. However, due to the binary nature of the feedback weights, a performance gap remains and further widens on more challenging tasks like CIFAR-100. Still, this work outlines the potential of SS in training deep SNNs for classification, which has never been explored in this context before. In Appendix B.2, we further study the impact of sign transport on our freezing mechanism. We show that, unlike sFA and SS, enforcing sign symmetry during training with FBP does not improve accuracy. Also, our freezing mechanism can successfully be applied to SS, suggesting that it may generalize beyond a specific BP-based algorithm.

Only little work in the literature has successfully directly trained TTFS-based deep SNNs [46, 13, 14, 6]. With ANN pretraining, Stanojevic et al. [6] reported state-of-the-art performance using VGG-16, achieving 93.27% on CIFAR-10 and 72.21% on CIFAR-100. Wei et al. [14] reported 91.17% on CIFAR-10 with VGG-11 and 69.66% with VGG-16 on CIFAR-100. In contrast, our results are obtained using only VGG-11 and no ANN pretraining, yet both our BP baseline and our FBP algorithm are competitive with state-of-the-art methods. The literature on TTFS-based SNNs with approaches targeting on-chip training remains limited to shallow networks [47, 28, 48, 29]. In [28], a 4-layer SNN achieved 92.80% on Fashion-MNIST; in [29], a 4-layer hybrid ANN-SNN achieved 79.5% on CIFAR-10 and 53.49% on CIFAR-100. Our work therefore establishes a baseline for TTFS-based deep SNNs trained with BP-based methods relaxing weight symmetry.

Table 1: Accuracy comparison between our method, FBP, and other feedback-driven methods.

Dataset	Architecture	Method	Transport Freq.		Epochs (Mean $\pm$ Std)	Accuracy (Mean $\pm$ Std %)
			Sign	Weight		
Fashion-MNIST	VGG-7	BP	1	1	110 $\pm$ 37	92.98 $\pm$ 0.21
		sFA	1	0	91 $\pm$ 23	92.50 $\pm$ 0.28
		SS	1	0	102 $\pm$ 33	92.75 $\pm$ 0.22
		FBP ( <i>ours</i> )	0.1	0.1	104 $\pm$ 32	92.99 $\pm$ 0.27
	VGG-11	BP	1	1	104 $\pm$ 28	92.98 $\pm$ 0.21
		sFA	1	0	89 $\pm$ 14	91.63 $\pm$ 0.46
		SS	1	0	94 $\pm$ 20	92.45 $\pm$ 0.22
		FBP ( <i>ours</i> )	0.1	0.1	76 $\pm$ 12	92.90 $\pm$ 0.16
CIFAR-10	VGG-7	BP	1	1	262 $\pm$ 34	90.40 $\pm$ 0.45
		sFA	1	0	298 $\pm$ 50	87.03 $\pm$ 0.69
		SS	1	0	334 $\pm$ 62	89.39 $\pm$ 0.66
		FBP ( <i>ours</i> )	0.1	0.1	295 $\pm$ 51	90.51 $\pm$ 0.64
	VGG-11	BP	1	1	245 $\pm$ 28	92.04 $\pm$ 0.51
		sFA	1	0	336 $\pm$ 77	89.48 $\pm$ 1.05
		SS	1	0	291 $\pm$ 55	91.26 $\pm$ 0.53
		FBP ( <i>ours</i> )	0.1	0.1	270 $\pm$ 59	92.04 $\pm$ 0.49
CIFAR-100	VGG-7	BP	1	1	308 $\pm$ 29	66.05 $\pm$ 0.42
		sFA	1	0	377 $\pm$ 61	60.97 $\pm$ 0.92
		SS	1	0	335 $\pm$ 44	63.43 $\pm$ 0.69
		FBP ( <i>ours</i> )	0.1	0.1	328 $\pm$ 46	65.76 $\pm$ 0.80
	VGG-11	BP	1	1	262 $\pm$ 49	67.45 $\pm$ 0.93
		sFA	1	0	381 $\pm$ 44	62.33 $\pm$ 0.75
		SS	1	0	289 $\pm$ 41	65.34 $\pm$ 0.79
		FBP ( <i>ours</i> )	0.1	0.1	291 $\pm$ 27	67.25 $\pm$ 0.62

### 4.3 Reducing the Number of Weights Transported

To reduce the total number of weights transported during training, two complementary methods can be employed: reducing the frequency of weight transports (via  $\Phi$ , the number of iterations with frozen feedback weights), or reducing the number of weights transported at a time (via partial weight transport, controlled by a strategy-specific hyperparameter). In Figure 2, we compare the accuracy drop against the weight transport reduction factor of FBP relative to BP, on VGG-11. The analysis includes our three partial transport strategies and various values of  $\Phi$ . To ensure a fair comparison in terms of computational effort, we train each FBP configuration for at most the number of epochs used by BP, stopping training if convergence is not reached within this limit. The transport reduction factor is computed as the ratio between the total number of weights transported in BP and FBP. The total number of weights is obtained by multiplying the number of transports during training by the number of weights transferred per transport. As a result, it depends on both  $\Phi$  and the specific hyperparameter of each partial weight transport strategy, which explains why the lines start and end at different positions along the x-axis. In Appendix B.3, we provide additional experimental details and supplementary results to further demonstrate the impact of the strategy-specific hyperparameters.

The solid black line shows the performance of the baseline: default FBP without partial weight transport, across varying  $\Phi$  values. For a given transport reduction factor, configurations that lie above this line achieve better accuracy at the same transport cost. As observed, *Random sampling* generally fails to outperform the FBP baseline. It shows marginal improvements only at low transport reduction levels, where either the probability of transporting each weight or the transport frequency is sufficiently high. Its limited effectiveness can be explained by the stochastic nature of the sampling, which requires frequent realignment to reliably correct larger biases. To address this, *Change-*

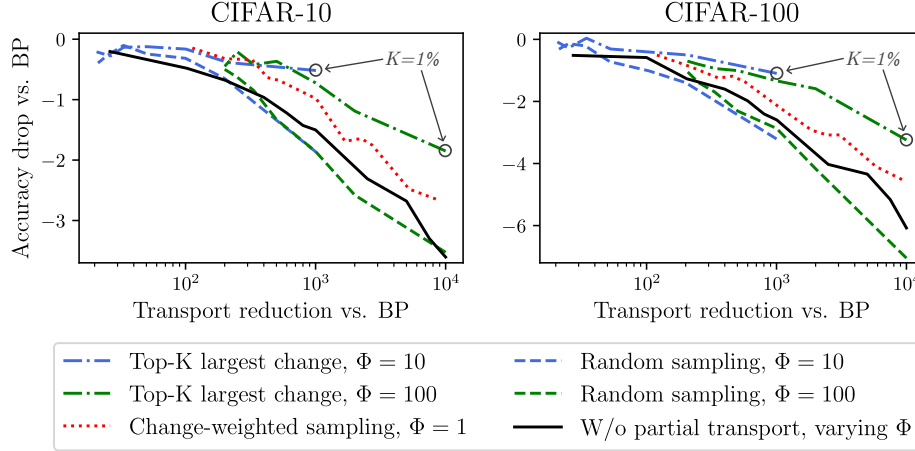


Figure 2: Accuracy drop versus weight transport reduction factor of FBP relative to BP, across different partial weight transport strategies and various number of frozen iterations  $\Phi$ . Each strategy is evaluated by varying its specific hyperparameter. The x-axis uses a logarithmic scale, and y-axis ranges are adapted for each dataset to improve visualization. Best seen in color.

*weighted sampling* assigns higher transport probabilities to weights with larger accumulated changes, improving accuracy over *Random sampling* and outperforming the FBP baseline. Also, it does not rely on a fixed transport interval ( $\Phi = 1$ ), allowing weights to be realigned as needed. The superior performance of this strategy highlights the importance of selection in partial weight transport.

Among all strategies, *Top-K largest change* achieves the best performance. This is because it explicitly corrects the largest weight biases. It remains effective even at high transport reduction levels, with as few as  $K = 1\%$  of weights transferred per transport. Thus, on CIFAR-10, it can reduce weight transport by  $1,000\times$  with a 0.52 pp accuracy drop (compared to 1.50 pp for default FBP), and by  $10,000\times$  with a 1.85 pp drop (3.61 pp for default FBP). Similarly, on CIFAR-100, it achieves a 1.10 pp drop with a  $1,000\times$  reduction (compared to 2.60 pp for default FBP), and a 3.24 pp drop with a  $10,000\times$  reduction (6.08 pp for default FBP). Note that accuracy drops can be further reduced by training until early stopping: we measure a drop of 1.15 pp on CIFAR-10 and 1.06 pp on CIFAR-100 with a  $8,093\times$  and a  $7,003\times$  reduction, respectively. While it remains unclear whether this strategy can be efficiently implemented on hardware, our goal is rather to demonstrate that transporting only a subset of the weights not only reduces the number of transports but also sufficiently corrects magnitude mismatches to support effective learning under relaxed weight symmetry.

#### 4.4 Impact of Weight Magnitude Mismatch

FBP aims to minimize the gradient bias introduced by the magnitude mismatch between forward and feedback weights. In this section, we quantify this bias by measuring the cosine similarity between true weight updates, computed using gradients based solely on forward weights (i.e., by replacing  $B$  with  $W$  in step 9 of Algorithm 1), and actual weight updates, relying on neuron errors propagated through feedback weights. Figure 3 shows this alignment throughout training on CIFAR-100 with VGG-11, across different feedback-driven methods. FBP maintains near-perfect alignment, even when combined with *Top-K largest change* partial transport at  $K = 1\%$ , consistently achieving higher cosine similarity compared to sFA and SS. This alignment explains its superior performance, as gradient directions remain more accurate throughout training. Interestingly, SS shows

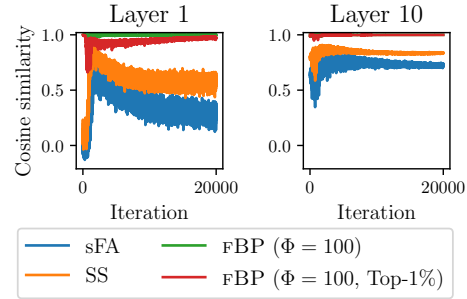


Figure 3: Cosine similarity between true and actual weight changes during training on CIFAR-100. Best seen in color.

higher similarity than sFA, despite its feedback weights being limited to the sign of the forward weights. This is also reflected empirically in its higher accuracy, suggesting that the stochasticity in sFA introduces directional noise in the gradient updates, leading to larger misalignment. Last, cosine similarity tends to decrease in early layers. This is because the magnitude mismatch between forward and feedback weights accumulates bias as gradients backpropagate through multiple layers. FBP is less affected than sFA and SS by this accumulated bias, potentially indicating better scalability to deeper networks. In Appendix B.4, we provide additional results with similar conclusions across other datasets and all trainable layers.

## 5 Discussion

In this paper, we improve training efficiency in dual-network configurations with our FBP algorithm and our partial weight transport scheme. Our results show that weight transport after every update is not necessary for near-optimal training, that transporting only a subset of the weights can sufficiently correct magnitude mismatches, and that enforcing sign symmetry during training provides no benefit when periodic weight transport is applied. These findings provide valuable insights to guide future efforts in the design of neuromorphic hardware with efficient BP-based on-chip learning.

FBP does not entirely eliminate the weight transport problem, as it still requires periodic synchronization. Instead, it provides a middle ground between full weight symmetry and fully decoupled feedback weights, similar to sFA and SS, which rely on sign transport. This can introduce design constraints, data movement overhead, and additional energy consumption on neuromorphic hardware. While FBP offers accuracy improvements over both sFA and SS, it requires additional transport of weight values along with the signs. A drawback of sFA and SS is that they transmit signs after each iteration, which may incur higher synchronization overhead than FBP. The limited support for BP-based deep learning in current neuromorphic hardware—often restricted to shallow architectures and local learning rules [20]—makes it difficult to measure the energy cost of transporting weights or signs. Thus, it remains uncertain whether more frequent sign transport offers a substantial efficiency advantage over weight transport. Other approaches rely on mechanisms to learn the feedback weights rather than transporting the forward weights to them [24, 22, 20]. Similar to FBP, these approaches require sharing neuron spike times and errors between networks. However, they also double (at least) the number of weight updates per iteration, increasing both computational and energy costs [49, 20]. At this stage, it is unclear which approach is best suited for BP-based training on neuromorphic hardware. The key challenge of FBP is to find the optimal trade-off between transport frequency and accuracy that makes its overhead practical for hardware implementation. This work does not claim our method to be the optimal solution, but rather seeks to provide insights for hardware design.

Theoretically, FBP is agnostic to network architecture and BP algorithm. Regarding architecture, it can be applied to any parameterized architecture requiring forward and feedback paths. Our method can be extended to other trainable parameters, such as biases or batch normalization parameters, as the transport mechanism applies identically. Regarding training algorithms, FBP does not change the form of the update equations but computes neuron errors using distinct weights. It is therefore compatible, in principle, with a wide range of BP-based methods for SNNs, including BPTT, and, more generally, with traditional BP for ANNs. The only requirement is that gradients must be backpropagated through the exact reverse circuit of the forward pass. However, freezing the feedback weights induces biased neuron errors. The more updates are performed with these biased errors, the more the learning trajectory may diverge. Thus, FBP may not adapt equally well to all algorithms, particularly those with dense updates, such as BPTT. Our experiment in Appendix B.2, where our freezing mechanism was applied to SS, suggested that FBP may generalize to other BP-based methods. Yet, further research is needed to determine under which conditions FBP remains effective.

FBP computes gradients using a stale version of the forward weights. This approach raises similarities with methods employing delayed gradients [50, 51], often encountered in asynchronous learning scenarios where workers compute gradients based on outdated model weights. However, FBP differs by separating forward and feedback weights (dual-network configuration), and by explicitly freezing the feedback weights for a given number of iterations (typically higher than in asynchronous learning). Still, these characteristics make FBP conceptually relevant to distributed [50] and federated [52] learning, which could inspire future work to draw from these domains, for example to mitigate the bias introduced by stale gradients [50, 51].

## Acknowledgments and Disclosure of Funding

This work is funded by Chaire Luxant-ANVI (Métropole de Lille) and supported by IRCICA (CNRS UAR 3380). Experiments presented in this paper were carried out using the Grid'5000 testbed [53], supported by a scientific interest group hosted by Inria and including CNRS, RENATER and several Universities as well as other organizations (see <https://www.grid5000.fr>). We would like to thank Alpha Renner, Andrew Sornborger, and Gabriel Béna for the useful exchanges regarding the training of SNNs on neuromorphic hardware. We also thank Wenjie Wei for providing the code from their paper, which our work builds upon.

## References

- [1] Kashu Yamazaki, Viet-Khoa Vo-Ho, Darshan Bulsara, and Ngan Le. Spiking Neural Networks and Their Applications: A Review. *MDPI Brain Sciences*, 12(7), 2022.
- [2] Catherine D. Schuman, Thomas E. Potok, Robert M. Patton, J. Douglas Birdwell, Mark E. Dean, Garrett S. Rose, and James S. Plank. A Survey of Neuromorphic Computing and Neural Networks in Hardware. *arXiv*, arXiv:1705.06963, 2017.
- [3] Peter Blouw, Xuan Choo, Eric Hunsberger, and Chris Eliasmith. Benchmarking Keyword Spotting Efficiency on Neuromorphic Hardware. In *Neuro-Inspired Computational Elements Workshop*, 2019.
- [4] Christoph Ostrau, Jonas Homburg, Christian Klarhorst, Michael Thies, and Ulrich Rückert. Benchmarking Deep Spiking Neural Networks on Neuromorphic Hardware. In *International Conference on Artificial Neural Networks*, 2020.
- [5] Alina Fedorova, Nikola Jovišić, Jordi Vallverdú, Silvia Battistoni, Miloš Jovičić, Milovan Medojević, Alexander Toshev, Evgeniia Alshanskaia, Max Talanov, and Victor Erokhin. Advancing Neural Networks: Innovations and Impacts on Energy Consumption. *Advanced Electronic Materials*, 10(12), 2024.
- [6] Ana Stanojevic, Stanisław Woźniak, Guillaume Bellec, Giovanni Cherubini, Angeliki Pantazi, and Wulfram Gerstner. High-Performance Deep Spiking Neural Networks with 0.3 Spikes Per Neuron. *Nature Communications*, 15(1), 2024.
- [7] Jason K. Eshraghian, Max Ward, Emre O. Neftci, Xinxin Wang, Gregor Lenz, Girish Dwivedi, Mohammed Bennamoun, Doo Seok Jeong, and Wei D. Lu. Training Spiking Neural Networks Using Lessons from Deep Learning. *Proceedings of the IEEE*, 111(9), 2023.
- [8] Yujie Wu, Lei Deng, Guoqi Li, Jun Zhu, and Luping Shi. Spatio-Temporal Backpropagation for Training High-Performance Spiking Neural Networks. *Frontiers in Neuroscience*, 12, 2018.
- [9] Yuhang Li, Tamar Geller, Youngeun Kim, and Priyadarshini Panda. SEENN: Towards Temporal Spiking Early Exit Neural Networks. In *Advances in Neural Information Processing Systems*, volume 36, 2023.
- [10] Guillaume Bellec, Franz Scherr, Anand Subramoney, Elias Hajek, Darjan Salaj, Robert Legenstein, and Wolfgang Maass. A Solution to the Learning Dilemma for Recurrent Networks of Spiking Neurons. *Nature Communications*, 11(1), 2020.
- [11] Lina Bonilla, Jacques Gautrais, Simon Thorpe, and Timothée Masquelier. Analyzing Time-to-First-Spike Coding Schemes: A Theoretical Approach. *Frontiers in Neuroscience*, 16, 2022.
- [12] Hesham Mostafa. Supervised Learning Based on Temporal Coding in Spiking Neural Networks. *IEEE Transactions on Neural Networks and Learning Systems*, 29, 2018.
- [13] Shibo Zhou, Xiaohua Li, Ying Chen, Sanjeev T. Chandrasekaran, and Arindam Sanyal. Temporal-Coded Deep Spiking Neural Network with Easy Training and Robust Performance. In *AAAI Conference on Artificial Intelligence*, volume 35, 2021.

- [14] Wenjie Wei, Malu Zhang, Hong Qu, Ammar Belatreche, Jian Zhang, and Hong Chen. Temporal-Coded Spiking Neural Networks with Dynamic Firing Threshold: Learning with Event-Driven Backpropagation. In *International Conference on Computer Vision*, 2023.
- [15] Seongsik Park, Seijoon Kim, Byunggook Na, and Sungroh Yoon. T2FSNN: Deep Spiking Neural Networks with Time-to-First-Spike Coding. In *Design Automation Conference*, 2020.
- [16] Rufin Van Rullen and Simon J. Thorpe. Rate Coding Versus Temporal Order Coding: What the Retinal Ganglion Cells Tell the Visual Cortex. *Neural Computation*, 13(6), 2001.
- [17] Daniel Auge, Julian Hille, Etienne Mueller, and Alois Knoll. A Survey of Encoding Techniques for Signal Processing in Spiking Neural Networks. *Neural Processing Letters*, 53(6), 2021.
- [18] Emre Neftci, Charles Augustine, Somnath Paul, and Georgios Detorakis. Event-Driven Random Back-Propagation: Enabling Neuromorphic Deep Learning Machines. *Frontiers in Neuroscience*, 11, 2017.
- [19] Friedemann Zenke and Emre Neftci. Brain-Inspired Learning on Neuromorphic Substrates. *Proceedings of the IEEE*, 109(5), 2021.
- [20] Alpha Renner, Forrest Sheldon, Anatoly Zlotnik, Louis Tao, and Andrew Sornborger. The Backpropagation Algorithm Implemented on Spiking Neuromorphic Hardware. *Nature Communications*, 15, 2024.
- [21] Stephen Grossberg. Competitive Learning: From Interactive Activation to Adaptive Resonance. *Cognitive Science*, 11, 1987.
- [22] Mohamed Akrouf, Collin Wilson, Peter Humphreys, Timothy Lillicrap, and Douglas B Tweed. Deep Learning without Weight Transport. In *Advances in Neural Information Processing Systems*, volume 32, 2019.
- [23] Qianli Liao, Joel Leibo, and Tomaso Poggio. How Important Is Weight Symmetry in Backpropagation? In *AAAI Conference on Artificial Intelligence*, volume 30, 2016.
- [24] Daniel Kunin, Aran Nayebi, Javier Sagastuy-Brena, Surya Ganguli, Jonathan Bloom, and Daniel Yamins. Two Routes to Scalable Credit Assignment without Weight Symmetry. In *International Conference on Machine Learning*, 2020.
- [25] Brian Crafton, Matt West, Padip Basnet, Eric Vogel, and Arijit Raychowdhury. Local Learning in RRAM Neural Networks with Sparse Direct Feedback Alignment. In *International Symposium on Low Power Electronics and Design*, 2019.
- [26] Jacques Kaiser, Hesham Mostafa, and Emre Neftci. Synaptic Plasticity Dynamics for Deep Continuous Local Learning (DECOLLE). *Frontiers in Neuroscience*, 14, 2020.
- [27] Tielin Zhang, Shuncheng Jia, Xiang Cheng, and Bo Xu. Tuning Convolutional Spiking Neural Network with Biologically Plausible Reward Propagation. *IEEE Transactions on Neural Networks and Learning Systems*, 33(12), 2021.
- [28] Maryam Mirsadeghi, Majid Shalchian, Saeed Reza Kheradpisheh, and Timothée Masquelier. Spike Time Displacement-Based Error Backpropagation in Convolutional Spiking Neural Networks. *Neural Computing and Applications*, 35(21), 2023.
- [29] Gaspard Goupy, Pierre Tirilly, and Ioan Marius Bilasco. Neuronal Competition Groups with Supervised STDP for Spike-Based Classification. In *Advances in Neural Information Processing Systems*, volume 37, 2024.
- [30] Florian Bacho and Dominique Chu. Low-Variance Forward Gradients Using Direct Feedback Alignment and Momentum. *Neural Networks*, 169, 2024.
- [31] Timothy P. Lillicrap, Daniel Cownden, Douglas B. Tweed, and Colin J. Akerman. Random Synaptic Feedback Weights Support Error Backpropagation for Deep Learning. *Nature Communications*, 7(1), 2016.

- [32] Arild Nøkland. Direct Feedback Alignment Provides Learning in Deep Neural Networks. In *Advances in Neural Information Processing Systems*, volume 29, 2016.
- [33] Will Xiao, Honglin Chen, Qianli Liao, and Tomaso Poggio. Biologically-Plausible Learning Algorithms Can Scale to Large Datasets. In *International Conference on Learning Representations*, 2019.
- [34] Dongcheng Zhao, Yi Zeng, Tielin Zhang, Mengting Shi, and Feifei Zhao. GLSNN: A Multi-Layer Spiking Neural Network Based on Global Feedback Alignment and Local STDP Plasticity. *Frontiers in Computational Neuroscience*, 14, 2020.
- [35] Amar Shrestha, Haowen Fang, Daniel Patrick Rider, Zaidao Mei, and Qinru Qiu. In-Hardware Learning of Multilayer Spiking Neural Networks on a Neuromorphic Processor. In *Design Automation Conference*, 2021.
- [36] Ping He, Rong Xiao, Chenwei Tang, Shudong Huang, Jiancheng Lv, and Huajin Tang. STSF: Spiking Time Sparse Feedback Learning for Spiking Neural Networks. *IEEE Transactions on Neural Networks and Learning Systems*, 2025.
- [37] Sergey Bartunov, Adam Santoro, Blake Richards, Luke Marris, Geoffrey E Hinton, and Timothy Lillicrap. Assessing the Scalability of Biologically-Motivated Deep Learning Algorithms and Architectures. In *Advances in Neural Information Processing Systems*, volume 31, 2018.
- [38] Theodore H. Moskovitz, Ashok Litwin-Kumar, and L. F. Abbott. Feedback Alignment in Deep Convolutional Networks. *arXiv*, arXiv:1812.06488, 2019.
- [39] Mingqing Xiao, Qingyan Meng, Zongpeng Zhang, Di He, and Zhouchen Lin. Hebbian Learning Based Orthogonal Projection for Continual Learning of Spiking Neural Networks. In *International Conference on Learning Representations*, 2024.
- [40] Han Xiao, Kashif Rasul, and Roland Vollgraf. Fashion-MNIST: A Novel Image Dataset for Benchmarking Machine Learning Algorithms. *arXiv*, arXiv:1708.07747, 2017.
- [41] Alex Krizhevsky. Learning Multiple Layers of Features from Tiny Images. Technical report, University of Toronto, 2009.
- [42] Yann LeCun, Léon Bottou, Yoshua Bengio, and Patrick Haffner. Gradient-Based Learning Applied to Document Recognition. *Proceedings of the IEEE*, 86(11), 1998.
- [43] Karen Simonyan and Andrew Zisserman. Very Deep Convolutional Networks for Large-Scale Image Recognition. *arXiv*, arXiv:1409.1556, 2015.
- [44] Kaiming He, Xiangyu Zhang, Shaoqing Ren, and Jian Sun. Delving Deep into Rectifiers: Surpassing Human-Level Performance on ImageNet Classification. In *International Conference on Computer Vision*, 2015.
- [45] Diederik P. Kingma and Jimmy Ba. Adam: A Method for Stochastic Optimization. In *International Conference on Learning Representations*, 2015.
- [46] Seongsik Park and Sungroh Yoon. Training Energy-Efficient Deep Spiking Neural Networks with Time-to-First-Spike Coding. *arXiv*, arXiv:2106.02568, 2021.
- [47] Milad Mozafari, Mohammad Ganjtabesh, Abbas Nowzari-Dalini, Simon J. Thorpe, and Timothée Masquelier. Bio-Inspired Digit Recognition Using Reward-Modulated Spike-Timing-Dependent Plasticity in Deep Convolutional Networks. *Pattern Recognition*, 94, 2019.
- [48] Gaspard Goupy, Pierre Tirilly, and Ioan Marius Bilasco. Paired Competing Neurons Improving STDP Supervised Local Learning in Spiking Neural Networks. *Frontiers in Neuroscience*, 18, 2024.
- [49] Tatsukichi Shibuya, Nakamasa Inoue, Rei Kawakami, and Ikuro Sato. Fixed-Weight Difference Target Propagation. *AAAI Conference on Artificial Intelligence*, 37, 2023.

- [50] Shuxin Zheng, Qi Meng, Taifeng Wang, Wei Chen, Nenghai Yu, Zhi-Ming Ma, and Tie-Yan Liu. Asynchronous Stochastic Gradient Descent with Delay Compensation. In *International Conference on Machine Learning*, 2017.
- [51] Huiping Zhuang, Yi Wang, Qinglai Liu, and Zhiping Lin. Fully Decoupled Neural Network Learning Using Delayed Gradients. *IEEE Transactions on Neural Networks and Learning Systems*, 33(10), 2022.
- [52] Ligeng Zhu, Hongzhou Lin, Yao Lu, Yujun Lin, and Song Han. Delayed Gradient Averaging: Tolerate the Communication Latency for Federated Learning. In *Advances in Neural Information Processing Systems*, volume 34, 2021.
- [53] Franck Cappello, Frédéric Desprez, Michel Daydé, Emmanuel Jeannot, Yvon Jégou, Stephane Lanteri, Nouredine Melab, Raymond Namyst, Pascale Primet, Olivier Richard, Eddy Caron, Julien Leduc, and Guillaume Mornet. Grid’5000: A Large Scale, Reconfigurable, Controlable and Monitorable Grid Platform. In *International Workshop on Grid Computing*, 2005.
- [54] Malu Zhang, Jiadong Wang, Jibin Wu, Ammar Belatreche, Burin Amornpaisannon, Zhixuan Zhang, Venkata Pavan Kumar Miriyala, Hong Qu, Yansong Chua, Trevor E. Carlson, and Haizhou Li. Rectified Linear Postsynaptic Potential Function for Backpropagation in Deep Spiking Neural Networks. *IEEE Transactions on Neural Networks and Learning Systems*, 33(5), 2022.
- [55] Saeed Reza Kheradpisheh and Timothée Masquelier. Temporal Backpropagation for Spiking Neural Networks with One Spike per Neuron. *International Journal of Neural Systems*, 30(6), 2020.

## A Baseline

In this appendix, we present the neural coding, neuron model, and event-driven BP algorithm used in this paper, adopted from the TTFS-based deep SNN proposed in [14]. This framework was selected for its state-of-the-art performance and training efficiency; the rationale behind this choice is further discussed in Appendix A.4.

### A.1 Neural Coding

For the input encoding layer, we use the TTFS temporal coding scheme, also referred to as first-spike or latency coding [11]. This scheme converts each input value  $x \in [0, 1]$  to a single spike time  $t(x)$ :

$$t(x) = T_w \cdot (1 - x), \quad (\text{A.1})$$

where  $T_w$  is the length of the permissible spike time window (set to 1 in this work). Consequently, the intensity of the value is encoded through latency: higher values correspond to lower latencies, and vice versa.

### A.2 Neuron Model

To simulate the dynamics of spiking neurons, we adopt the ReL-PSP neuron model [54], which can be viewed as an Integrate-and-Fire (IF) model with linear post-synaptic potential function. Unlike simple IF neurons with instantaneous synapses [55], the membrane potential of ReL-PSP neurons increases continuously and linearly over time after receiving an input spike, even in the absence of subsequent spikes. The membrane potential  $V_j^l$  of neuron  $n_j^l$  in layer  $l$  is expressed as:

$$V_j^l(t) = \sum_{i=1}^{N^{l-1}} W_{ij}^l \cdot \epsilon(t - t_i^{l-1}), \quad (\text{A.2})$$

where  $t$  is the current time,  $N^{l-1}$  is the number of neurons in layer  $l - 1$ ,  $t_i^{l-1}$  is the spike time of neuron  $n_i^{l-1}$ ,  $W_{ij}^l$  is the weight of the synapse from  $n_i^{l-1}$  to  $n_j^l$ , and  $\epsilon(\cdot)$  is the kernel function, defined as:

$$\epsilon(t - t_i^{l-1}) = \begin{cases} t - t_i^{l-1} & \text{if } t > t_i^{l-1} \\ 0 & \text{o.w.} \end{cases}. \quad (\text{A.3})$$

When  $V_j^l$  reaches a threshold  $\theta$  at time  $t$  (i.e.,  $V_j^l(t) \geq \theta$ ),  $n_j^l$  emits a spike ( $t_j^l = t$ ), resets its membrane potential to zero, and remain deactivated until the next sample is shown. Consequently, aligned with TTFS coding, ReL-PSP neurons can fire at most once per sample and encode the intensity of their activation through spike timing: neurons firing first are the most strongly activated.

To define the thresholds of the neurons, we employ Dynamic Firing Threshold (DFT) [14]. In this method, the threshold  $\theta^l$  of layer  $l$  is modeled as a layer-dependent, time-varying function, linearly decreasing over time:

$$\theta^l(t) = \begin{cases} T_w \cdot (l+1) - t, & \text{if } T_w \cdot l \leq t \leq T_w \cdot (l+1) \\ +\infty & \text{o.w.} \end{cases} \quad (\text{A.4})$$

The encoding layer described in Appendix A.1 is regarded as the 0-th layer. With this method, neurons in the  $l$ -th layer can only fire within the spike time window  $[T_w \cdot l, T_w \cdot (l+1)]$ , ensuring that spikes do not overlap across layers.

Based on Equation A.2 and Equation A.4, the spike time of the neurons has a closed-form solution:

$$t_j^l = \begin{cases} T_w \cdot l & \text{if } V_j^l(T_w \cdot l) \geq \theta^l(T_w \cdot l) \\ \frac{T_w \cdot (l+1) + \sum_{i \in C_j^l} W_{ij}^l \cdot t_i^{l-1}}{1 + \sum_{i \in C_j^l} W_{ij}^l} & \text{if } T_w \cdot l < t_j^l \leq T_w \cdot (l+1) \\ +\infty & \text{o.w.} \end{cases} \quad (\text{A.5})$$

where  $C_j^l$  is the causal set<sup>1</sup> of neuron  $n_j^l$ .

### A.3 Event-Driven BP

The ReL-PSP neuron model described in Appendix A.2 enables exact gradient computation with respect to spike times [54, 6]. Hence, event-driven BP can be employed to train the SNN [14]. Since neurons encode the intensity of their activation through spike timing, we aim for the target neuron to fire first, while all others fire as late as possible. To achieve this, we apply a cross-entropy loss to the negated spike times of the output layer  $L$ :

$$\mathcal{L}(t^L, d) = -\log \frac{\exp(-t_d^L)}{\sum_{i=1}^M \exp(-t_i^L)}, \quad (\text{A.6})$$

where  $\mathcal{L}$  is the loss function,  $M$  is the number of output neurons ( $M$  is equal to the number of classes), and  $d$  is the target class index (ground-truth label).

We compute the derivative of the loss with respect to the weights following Equation 1. The gradient  $\frac{\partial \mathcal{L}}{\partial t^L}$  is obtained directly from the loss function in Equation A.6. BP then proceeds by iteratively computing, based on Equation A.5, the derivatives at layer  $l$  of the output spike time  $t_j^l$  with respect to the weight  $W_{ij}^l$  and the input spike times  $t_i^{l-1}$ :

$$\frac{\partial t_j^l}{\partial W_{ij}^l} = \begin{cases} \frac{t_i^{l-1} - t_j^l}{1 + \sum_{i \in C_j^l} W_{ij}^l} & \text{if } T_w \cdot l < t_j^l < T_w \cdot (l+1) \\ 0 & \text{o.w.} \end{cases}, \quad (\text{A.7})$$

$$\frac{\partial t_j^l}{\partial t_i^{l-1}} = \begin{cases} \frac{W_{ij}^l}{1 + \sum_{i \in C_j^l} W_{ij}^l} & \text{if } T_w \cdot l < t_j^l < T_w \cdot (l+1) \\ 0 & \text{o.w.} \end{cases}. \quad (\text{A.8})$$

### A.4 Motivations for the Baseline

TTFS coding and the ReL-PSP model impose a single-spike constraint, effectively reducing the number of generated spikes. This inherent spike sparsity makes the SNN particularly attractive for ultra-low-power applications. Beyond efficiency, the ReL-PSP model enables exact gradient computation with respect to spike times [54, 6], allowing direct application of event-driven BP. However, only a few TTFS-based methods have scaled effectively to deep networks [46, 13, 14, 6]. The key components we identify for successful scalability are:

<sup>1</sup>Assuming an output neuron  $n_j$  fires at  $t_j$ , the causal set  $C_j = \{n_i : t_i < t_j\}$  is the subset of input neurons that fire before  $n_j$ .

- a) *Controlled sparsity*—Excessive sparsity must be avoided to ensure spike propagation in deeper layers and to prevent the dead neuron problem [7] during BP. The ReL-PSP model addresses this issue by enabling membrane potentials to increase continuously over time, even in the absence of further input spikes [54]. The DFT mechanism further promotes spike generation by progressively lowering thresholds over the spike time window of the neurons [14].
- b) *Simulation and training speed*—The analytical expression for spike times (cf. Equation A.5) enables GPU-based training of the SNN in a manner analogous to an ANN, without requiring simulation over multiple time steps. Additionally, applying layer-dependent firing constraints, where neurons in layer  $l$  cannot fire before neurons in layer  $l - 1$ , eliminates the need to explicitly compute the causal set [14, 6], which is computationally expensive.
- c) *Parameter initialization*—Training deeper networks is more challenging, particularly due to parameter initialization. While ANN pretraining has been proposed as a solution [14, 6], we deliberately avoid it to maintain a fully spike-based training pipeline. This choice limits our ability to scale to deeper architectures such as VGG-16 [14, 6].

## B Additional Results

### B.1 Experimental Details

#### B.1.1 Datasets

Fashion-MNIST is available at <https://github.com/zalandoresearch/fashion-mnist> under the MIT license. CIFAR-10 and CIFAR-100 are available at <https://www.cs.toronto.edu/~kriz/cifar.html> under the MIT license.

#### B.1.2 Computing Resources

Experiments were conducted on private servers equipped with Nvidia A100 GPUs (40 GiB) and running Debian Linux. Code was implemented in Python 3.9 using PyTorch. The total runtime depends on several factors, such as the dataset, architecture, batch size, and number of epochs. For example, training a VGG-11 on CIFAR-100 with BP took approximately 15 seconds per epoch with a batch size of 256 (6.9 GiB memory usage) and 20 seconds per epoch with a batch size of 32 (1.5 GiB memory usage). The entire experimentation process spanned four months, yielding over 5,000 runs (i.e., training of a single model), including gridsearches and runs with random holdout splits.

### B.2 Impact of Sign Transport

In this work, we employ periodic weight transport between the forward and the feedback weights to minimize magnitude mismatch and preserve gradient direction. However, this approach can also be reduced to transport solely the signs of the weights. In this appendix, we study the impact of sign transport on our freezing mechanism.

In Figure B.1, we evaluate, on the VGG-11 architecture, the accuracy drop of FBP-based methods relative to BP, across different values of  $\Phi$ . Each variant is introduced in the appendix as it becomes relevant to the discussion. To ensure a fair comparison in terms of computational effort, we train each FBP-based method for the same number of epochs as BP. This implies that FBP reduces weight transport by a factor of  $\Phi$  relative to BP. In this experiment, we reduce the batch size to 32 and adjust the initial learning rate to  $3 \times 10^{-5}$  (fine-tuned with gridsearch on the validation set of CIFAR-10, for BP training). This setting allows us to validate our method with a different batch size and to approximate an online learning scenario, which is more relevant for on-chip training on neuromorphic hardware. For reference, with this setting, BP achieved  $92.99 \pm 0.24$  on Fashion-MNIST,  $92.10 \pm 0.38$  on CIFAR-10, and  $68.36 \pm 0.47$  on CIFAR-100.

**FBP** Globally, the need for frequent weight transport grows with the complexity of the task: on Fashion-MNIST, default FBP (without partial weight transport) maintains near-optimal accuracy regardless of  $\Phi$ , whereas on CIFAR-100, higher  $\Phi$  leads to larger accuracy drops. Compared to Section 4.2,  $\Phi$  can be increased with small performance degradation. With  $\Phi = 1000$ , FBP can reduce weight transport by  $1,000\times$  while maintaining accuracy within 0.21, 1.50, and 2.60 pp of BP

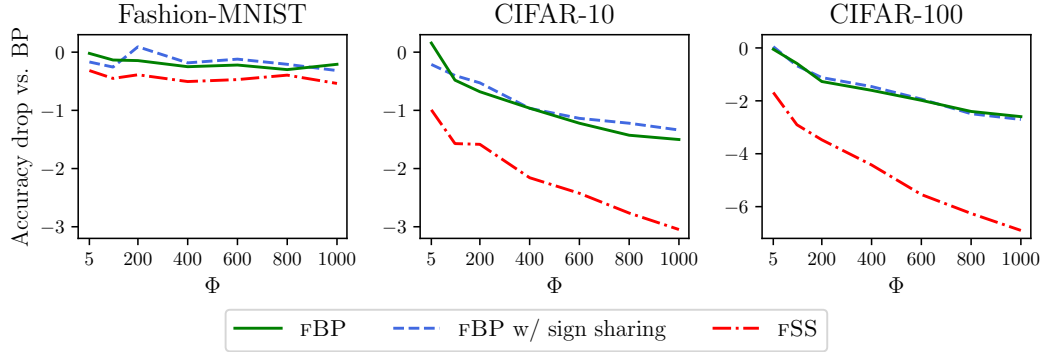


Figure B.1: Accuracy drop of various methods with frozen feedback weights relative to BP, evaluated on VGG-11 for varying number of iterations  $\Phi$ . The y-axis range of the CIFAR-100 plot is larger to accommodate greater accuracy drops. Best seen in color.

on Fashion-MNIST, CIFAR-10, and CIFAR-100, respectively. We demonstrated in Section 4.3 that our partial weight transport scheme can further reduce accuracy drops under high transport reduction.

**FBP with Sign Sharing** Prior work [23, 33] showed that enforcing sign symmetry is critical for scalability to deeper networks, motivating the development sFA and SS. To assess the specific contribution of sign symmetry in FBP, we also evaluate it with sign sharing in Figure B.1. In this variant, the forward and feedback weights share the same signs, similarly to sFA and SS. Specifically, at every iteration, the signs of the forward weights are copied to the feedback weights. Weight transport (to correct magnitude mismatches) proceeds as in default FBP, occurring at fixed intervals. Note that sign sharing incurs additional transport costs not accounted for here, leading to a biased comparison but enabling a more accurate evaluation of its impact on performance. Our results show that incorporating sign sharing has no significant effect on the accuracy achieved by FBP, even at low transport frequencies (i.e., for higher values of  $\Phi$ ). This is likely because weight transport naturally corrects sign mismatches, although occurring at fixed intervals. During these intervals, temporary sign mismatches may arise, but their impact remains limited. Indeed, when a weight flips its sign during training, its magnitude is typically low both before and after the change. Thus, forward and feedback weights may have opposite signs but remain small in magnitude, leading to negligible influence on both neuron activations and backpropagated errors. We conclude that sign correction can be safely delayed until the next scheduled weight transport without affecting training.

**FSS** We state in the paper that freezing feedback weights is agnostic to the specific BP algorithm. Here, we evaluate the relevance of our freezing mechanism when applied to SS. We refer to this variant as FSS (frozen SS). In this case, weight signs are transported after  $\Phi$  iterations instead of every iteration, reducing the frequency of sign transport. Figure B.1 shows that FSS successfully supports training with our frozen feedback weights, suggesting that our method may generalize beyond a specific BP-based algorithm. However, FBP outperforms it across all datasets. In addition, the accuracy of FSS degrades more rapidly than FBP as  $\Phi$  increases. This highlights that our freezing mechanism is less effective in SS than in BP, likely because SS already imposes a strong constraint by limiting feedback weights to binary values, making it more sensitive to outdated feedback weights. These results confirm that reducing magnitude mismatches between forward and feedback weights is important to mitigating gradient bias and achieving more effective learning in deep SNNs.

### B.3 Reducing the Number of Weights Transported

#### B.3.1 Experimental Details

We provide additional experimental details related to the experiments in Section 4.3. In Figure 2, we evaluate *Change-weighted sampling* only with  $\Phi = 1$  because the strategy operates without a fixed interval (see Section 3.2). For *Random sampling* and *Top-K largest change*, we use  $\Phi = 10$  and  $\Phi = 100$ , as these values provide strong baselines with minimal accuracy degradation in the absence of partial weight transport. For FBP without partial weight transport (baseline), we consider values

of  $\Phi$  ranging from 25 to 10,000. As in the experiments of Appendix B.2, we reduce the batch size to 32 and adjust the initial learning rate to  $3 \times 10^{-5}$  (fine-tuned with gridsearch on the validation set of CIFAR-10, for BP training). Although this setting is more demanding in terms of computation time, it is motivated by two factors. First, it provides a more realistic analysis by approximating an online learning scenario, which is more relevant for on-chip training on neuromorphic hardware. Second, it allows us to validate our method under a different batch size, complementing the quantitative results in Section 4.2, which used a batch size of 256.

### B.3.2 Impact of Hyperparameters

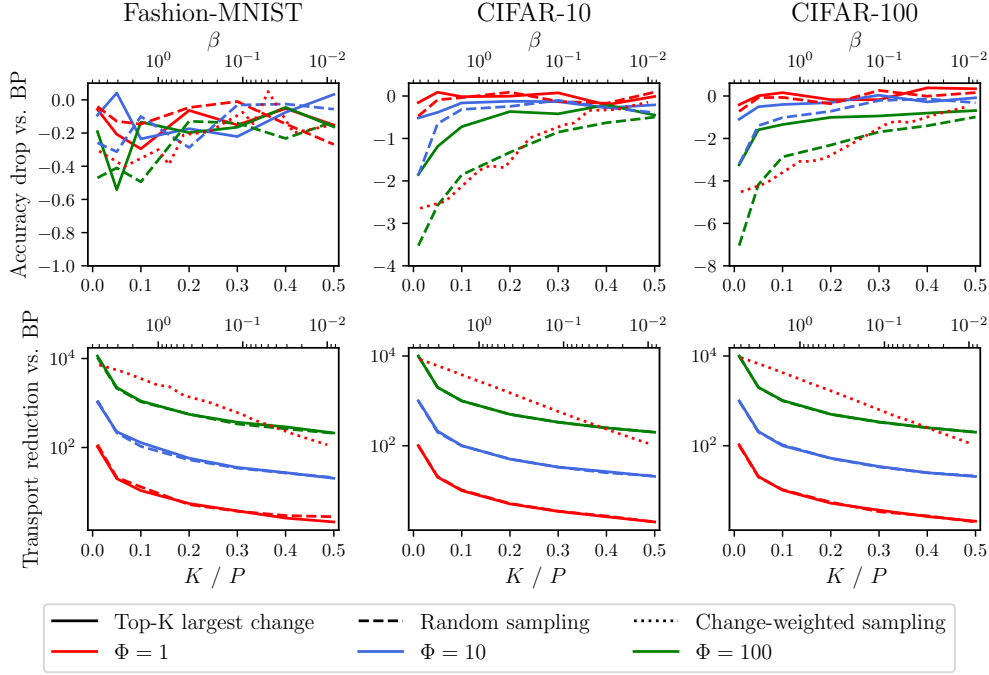
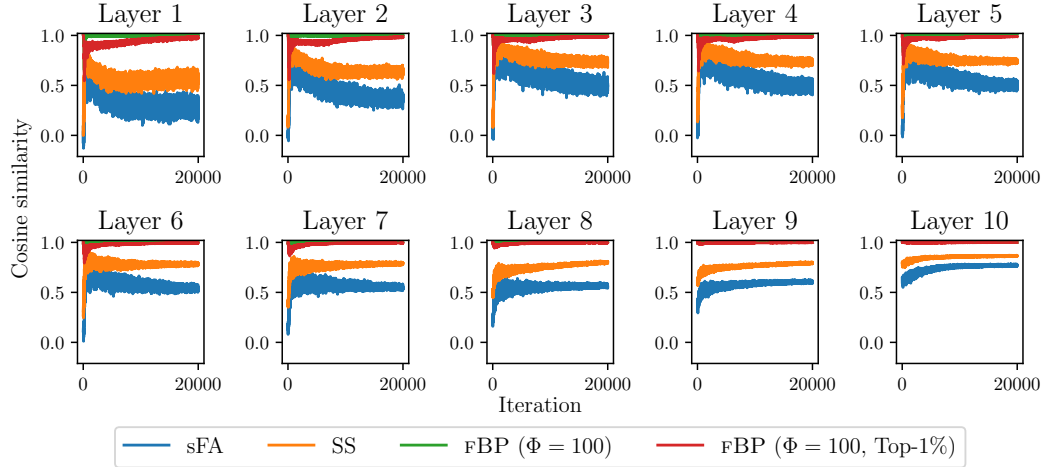
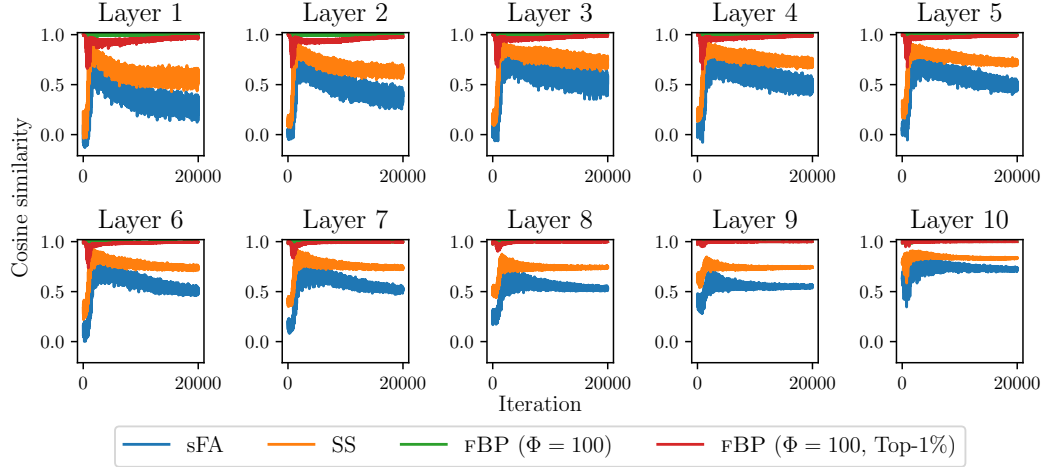


Figure B.2: Accuracy drop versus weight transport reduction factor of FBP relative to BP on VGG-11, for different partial weight transport strategies and varying number of iterations  $\Phi$ . The top x-axis is logarithmic, and the y-axis ranges differ for each dataset to enhance visualization. Best seen in color.

We showed in Section 4.3 that the total number of weights transported during training can be reduced by lowering the transport frequency (via  $\Phi$ ) and/or the number of weights transported at a time (via partial weight transport). We introduced three partial weight transport strategies, each controlled by a distinct hyperparameter. In this appendix, we provide additional visualizations across all datasets to illustrate the effect of these hyperparameters. Figure B.2 presents the accuracy drop versus weight transport reduction factor of FBP relative to BP, for our different partial weight transport strategies. FBP is trained for the same number of epochs as BP, ensuring fair comparison. This figure uses the same results as Figure 2, but splits them into separate plots for accuracy drop and transport reduction to better highlight the influence of the method-specific hyperparameters. *Top-K largest change* controls transport efficiency through  $\Phi$  and the top  $K\%$  of weights selected (bottom x-axis), *Random sampling* through  $\Phi$  and a sampling probability  $P$  (bottom x-axis), and *Change-weighted sampling* through a single temperature hyperparameter  $\beta$  (top x-axis). For simplicity, we use the same ranges for  $P$  and  $K$  across all values of  $\Phi$ . We additionally include results for  $\Phi = 1$  with *Top-K largest change* and *Random sampling*, compared to Figure 2. *Top-K largest change* and *Random sampling* require joint tuning of their respective hyperparameters to effectively improve transport reduction, whereas *Change-weighted sampling* relies on a single hyperparameter, making it easier to balance accuracy and efficiency.



(a) CIFAR-10



(b) CIFAR-100

Figure B.3: Cosine similarity between true and actual weight changes during training with VGG-11. Best seen in color.

#### B.4 Impact of Weight Magnitude Mismatch

In Section 4.4, we quantified the gradient bias introduced by the magnitude mismatch between forward and feedback weights. To do so, we measured the cosine similarity between true weight updates, computed using gradients based solely on forward weights (i.e., by replacing  $B$  with  $W$  in step 9 of Algorithm 1), and actual weight updates, relying on neuron errors propagated through feedback weights. We showed that FBP maintains near-perfect alignment, consistently achieving higher cosine similarity compared to sFA and SS. Here, we provide additional figures on CIFAR-10 (Figure B.3a) and CIFAR-100 (Figure B.3b) across all trainable layers. Note that “layer” refers to trainable layers only. Also, the last fully-connected layer is excluded because all methods receive the same neuron errors, resulting in identical weight changes. These results highlight that cosine similarity tends to decrease in early layers due to accumulated gradient bias during the BP phase. FBP is less impacted than sFA and SS by this accumulated bias, which could indicate better scalability to deeper networks.